Mm-Wave MIMO Channel Modeling and User Localization Using Sparse Beamspace Signatures

Hua Deng and Akbar Sayeed
Electrical and Computer Engineering, University of Wisconsin-Madison
Email: hdeng2@wisc.edu , akbar@engr.wisc.edu

***Abstract*—Millimeter-wave (mm-wave) communication systems operating between 30GHz and 300GHz are emerging as a promising technology for meeting the exploding bandwidth requirements of future wireless systems. In addition to large bandwidths, mm-wave systems afford high-dimensional multiple input multiple output (MIMO) operation with relatively compact arrays, and the corresponding narrow spatial beams make beamspace MIMO communication particular attractive. An important implication is that while the ambient spatial dimension is high, mm-wave MIMO channels exhibit a low-rank structure that is manifested in the sparsity of the beamspace MIMO channel matrix. In this paper, we develop a model for sparse mm-wave MIMO channels and propose an approach to mobile station (MS) localization that exploits changes in statistics of the sparse beamspace channel matrix as a function of the MS position. Unlike most existing methods, line-of-sight (LoS) propagation is not mandatory and the proposed approach benefits from the information provided by non-line-of-sight (NLoS) paths. Beamspace sparsity is exploited for developing a low-dimensional maximum-likelihood (ML) classifier that delivers near-optimal performance with dramatically reduced complexity compared to conventional designs. Numerical results illustrate the impact of the physical environment, grid-resolution, and MIMO dimensions on localization performance.**

***Index Terms*—Millimeter-Wave Communication, Massive MIMO, Sparse Channel Signature, Mobile Localization.**

I. Introduction

The rapid proliferation of wireless devices such as smartphones and tablets is leading to exponential growth in data rates and causing a spectrum crisis. At existing frequencies, small-cell technology is being explored for meeting this challenge by increasing the spatial re-use of the limited spectrum. MIMO techniques are also promising for interference management and spectral efficiency. Mm-wave systems offer a promising and complementary route to achieving the 1000-fold increase in aggregate data rates, predicted in the next decade, due to the larger available bandwidth as well as the high-dimensional MIMO operation [1]. Due to the quasi-optical nature of propagation, mm-wave communication is dominated by LoS paths and few dominant single-bounce NLoS paths, resulting in sparse channel characteristics [2], [3]. Recently, a framework for beamspace MIMO communication has been proposed that exploits beamspace channel sparsity and analog multi-beamforming for near-optimal performance with dramatically lower transceiver complexity compared to conventional MIMO approaches [3]–[6].

In this paper, we build on this work to develop a model for sparse MIMO channels, appropriate for mm-wave frequencies, and propose an approach for mobile station (MS) localization based on changes in the second-order statistics and sparsity patterns of the beamspace MIMO channel matrix as a function of MS position. Localization based on wireless channel signatures has a wide range of applications. Most existing techniques focus on the information provided by the LoS path, including angle of arrival (AoA), time difference of arrival (TDoA) or the received signal strength (RSS) [7]. However, LoS propagation is not always guaranteed in a real-world environment, e.g. urban or indoor settings. Furthermore, the presence of NLoS paths degrades the localization performance of current techniques and many methods have been proposed to alleviate the impact of NLoS propagation [8]. Other approaches that benefit from NLoS paths are proposed in [9], [10] for better channel estimation, but LoS path is still needed. In contrast to most existing algorithms, our approach benefits from the information provided by NLoS paths, and the presence of LoS path is not necessary.

In Sec. II we outline the physical environment and develop the sparse MIMO channel model and its beamspace representation as a function of MS location. Sec. III discusses the low-rank beamspace MIMO channel statistics induced by the channel sparsity mask. In Sec. IV, the MS localization problem is formulated as a multi-hypothesis classification problem. The sparsity of beamspace MIMO channel matrix is exploited to develop a low-complexity ML classifier that delivers near-optimal performance with dramatically reduced complexity. Representative numerical results are provided to illustrate the impact of physical environment, localization grid resolution, and MIMO dimension on classifier performance. Concluding remarks are provided in Sec. V.

II. Physical and Beamspace Channel Modeling

This section develops the MIMO channel model that serves as the basis for MS localization. The model captures the changes in second-order channel statistics as a function of MS location, and the beamspace MIMO representation reveals the sparse channel structure. A similar model is used in [11] for estimating the MS location from estimates of NLoS path parameters. In contrast, our approach exploits changes in the sparse channel statistics as a function of MS location.

A. Physical Channel Model

Consider a frequency non-selective MIMO system equipped with one-dimensional uniform linear array (ULAs) with N_t and N_r antennas at MS and BS (base station), respectively.

This work is partially supported by the US NSF Grant 1247583.

The transmitted and received signals are related as

$$\boldsymbol{r} = \boldsymbol{H}\boldsymbol{x} + \boldsymbol{w} \tag{1}$$

where $\boldsymbol{x}$ is the N_t-dimensional antenna domain transmitted signal (from the MS), $\boldsymbol{r}$ is the N_r-dimensional received signal (at the BS), $\boldsymbol{H}$ is the $N_r \times N_t$ channel matrix coupling the MS and BS arrays, and $\boldsymbol{w}$ is the white Gaussian noise. The MIMO channel matrix can be accurately modeled as

$$\boldsymbol{H} = \sum_{\ell=0}^{N_p} |\beta_\ell| e^{j\phi_\ell} \boldsymbol{a}_r(\theta_{r,\ell}) \boldsymbol{a}_t^H(\theta_{t,\ell}) \tag{2}$$

where N_p denotes the number of propagation paths, $\theta_{r,\ell}$ and $\theta_{t,\ell}$ are the angles seen by the BS and MS, respectively, and $|\beta_\ell|$ and ϕ_ℓ represent the amplitude and phase for the ℓ-th path. The LoS path corresponds to $\ell = 0$. The response vector $\boldsymbol{a}_r(\theta_{r,\ell})$ and steering vector $\boldsymbol{a}_t(\theta_{t,\ell})$ are given by

$$\boldsymbol{a}_r(\theta_{r,\ell}) = \frac{1}{\sqrt{N_r}}[a_{r,1}(\theta_{r,\ell}), \cdots, a_{r,N_r}(\theta_{r,\ell})]^T \tag{3}$$

$$\boldsymbol{a}_t(\theta_{t,\ell}) = \frac{1}{\sqrt{N_t}}[a_{t,1}(\theta_{t,\ell}), \cdots, a_{t,N_t}(\theta_{t,\ell})]^T \tag{4}$$

The elements of response/steering vector and normalized spatial angles $\theta_{r,\ell}$ and $\theta_{t,\ell}$ are given by

$$\begin{aligned} a_{r,i}(\theta_{r,\ell}) &= e^{-j2\pi\theta_{r,\ell}(i-1)}\ ,\ \theta_r = \frac{d_r}{\lambda}\sin(\alpha_{r,\ell}) \\ a_{t,i}(\theta_{t,\ell}) &= e^{-j2\pi\theta_{t,\ell}(i-1)}\ ,\ \theta_t = \frac{d_t}{\lambda}\sin(\alpha_{t,\ell}) \end{aligned} \tag{5}$$

where λ is the wavelength, $\alpha_{r,\ell}$ and $\alpha_{t,\ell}$ are the physical angles and d_r and d_t the antenna spacing at the BS and MS, respectively. In this paper, we assume $d_r = d_t = \lambda/2$.

According to the physical model (2), there are four parameters for each path: $|\beta_\ell|$, ϕ_ℓ, $\theta_{r,\ell}$ and $\theta_{t,\ell}$. We next discuss how these parameters depend on the MS location relative to the scatterers. We only consider the LoS path and single-bounce NLoS scattering paths since higher-order bounces suffer too much attenuation at mm-wave frequencies [2].

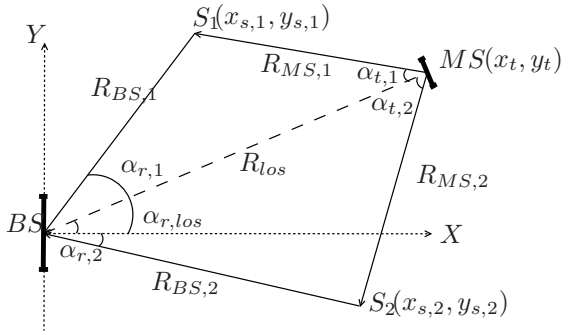

Fig. 1: Geometrical relation between BS and MS.

The geometrical relation between the BS and MS relative to the propagation paths is shown in Fig. 1. We fix the BS position as the origin, and the broadside direction as positive x-axis. The MS is always assumed facing the BS. Scattering objects are located between the BS and the MS in the area: $\{(x_s, y_s) : 50m \le x \le 150m\ ,\ -50m \le y \le 50m\}$.

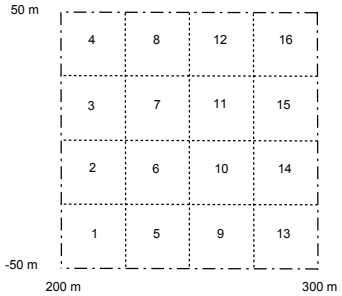

Fig. 2: Cell numbering

As shown in Fig. 2, we define the moving area for MS as $(x_t, y_t) \in [200m, 300m] \times [-50m, 50m]$ and split it into 16 disjoint cells ($25m \times 25m$) for the default case.

1) Angle of Departure (AoD) and Angle of Arrival (AoA): Since the MS is always facing the BS, for the LoS path ($\ell = 0$), the AoD at the MS is always zero ($\alpha_{t,los} = 0$), and the AoA at the BS ($\alpha_{r,los}$) is defined relative to the x-axis. For a particular NLoS scattering path ($\ell = 1, \cdots, N_p$), we define the AoD ($\alpha_{t,\ell}$) as the angle between the outgoing wave direction (from the MS) and LoS path direction, and the AoA ($\alpha_{r,\ell}$) at the BS as the angle between scattered wave direction and the positive x-axis. The AoDs and AoAs, $\{(\alpha_{r,\ell}, \alpha_{t,\ell})\}$, can be computing by using the geometrical relationship between the MS and scatterer locations relative to the BS; Fig. 1. The normalized AoAs and AoDs are computed via (5).

2) Path Amplitude and Phase: For a given MS position, (x_t, y_t), the phase for the LoS path ($\ell = 0$) is given by

$$\phi_\ell(x_t, y_t) = \phi_{los}(x_t, y_t) = \frac{2\pi R_{los}}{\lambda} = \frac{2\pi}{\lambda}\sqrt{{x_t}^2 + {y_t}^2}\ . \tag{6}$$

Similarly, for the same MS position, and for a given scatterer position, $(x_{s,\ell}, y_{s,\ell})$, the phase for the corresponding NLoS path ($\ell = 1 \cdots N_p$) can be computed as

$$\phi_\ell(x_t, y_t; x_{s,\ell}, y_{s,\ell}) = \frac{2\pi}{\lambda}\left(R_{BS,\ell} + R_{MS,\ell}\right) \tag{7}$$

where $R_{BS,\ell} = \sqrt{x_{s,\ell}^2 + y_{s,\ell}^2}$ is the distance from the BS to the scatterer and $R_{MS,\ell} = \sqrt{(x_t - x_{s,\ell})^2 + (y_t - y_{s,\ell})^2}$ is the distance from the scatterer to the MS; see Fig. 1.

The path loss for the LoS path ($\ell = 0$) is given by: $|\beta_0|^2 = G_t G_r \left(\frac{\lambda}{4\pi R_{los}}\right)^2$, and the path for single-bounce NLoS paths ($\ell \ge 1$) can be calculated as [12]

$$|\beta_\ell|^2 = \frac{P_{r,\ell}}{P_{t,\ell}} = \frac{G_t G_r \sigma}{(4\pi)^3}\left(\frac{\lambda}{R_{BS,\ell} R_{MS,\ell}}\right)^2 \tag{8}$$

where $P_{r,\ell}$ and $P_{t,\ell}$ are the power of received and transmitted signals, G_r and G_t are the antenna gains of BS and MS arrays, respectively, and σ represents the radar cross section which depends on the properties of scatterer and scattering angles. In simulations, we simply set $\sigma = 1$ for NLoS paths. Furthermore, prompted by recent measurements [2], we scale the LoS vs NLoS gains so that the NLoS path gains are 5-10dB weaker than the LoS path gain.

B. Beamspace MIMO Channel Representation

The physical model (2) depends on AoA and AoD in a non-linear manner. The beamspace MIMO channel representation is a linear representation of $\boldsymbol{H}$ with respect to uniformly spaced *virtual AoAs and AoDs* [13]:

$$\begin{aligned}\boldsymbol{H} &= \frac{1}{\sqrt{N_r N_t}} \sum_{i=1}^{N_r} \sum_{k=1}^{N_t} \boldsymbol{H}_b(i,k) \boldsymbol{a}_r(i\Delta\theta_r) \boldsymbol{a}_t^H(k\Delta\theta_t) \\ &= \boldsymbol{U}_r \boldsymbol{H}_b \boldsymbol{U}_t^H \quad \Leftrightarrow \quad \boldsymbol{H}_b = \boldsymbol{U}_r^H \boldsymbol{H} \boldsymbol{U}_t \end{aligned} \tag{9}$$

where $\boldsymbol{U}_r$ and $\boldsymbol{U}_t$ are unitary Discrete Fourier Transform (DFT) matrices whose columns are orthogonal response/steering vectors:

$$\boldsymbol{U}_r = \boldsymbol{U}_{r,dft} = \frac{1}{\sqrt{N_r}} [\boldsymbol{a}_r(i\Delta\theta_R)]_{i\in\mathcal{I}(N_r)} \tag{10}$$

$$\boldsymbol{U}_t = \boldsymbol{U}_{t,dft} = \frac{1}{\sqrt{N_t}} [\boldsymbol{a}_t(i\Delta\theta_t)]_{i\in\mathcal{I}(N_t)} \tag{11}$$

where $\mathcal{I}(n) = \{1, 2, \cdots, n\}$. The spacing between adjacent virtual AoAs and AoDs is determined by the BS and MS array resolution: $\Delta\theta_r = 1/N_r$ and $\Delta\theta_t = 1/N_t$. The beamspace channel matrix $\boldsymbol{H}_b$ in (9) is a unitarily equivalent representation of the antenna domain channel matrix $\boldsymbol{H}$.

III. Sparse Beamspace Channel Statistics

We now discuss the beamspace channel statistics and sparse signatures that capture the MS location information.

A. Channel Statistics and Sparsity Masks

We construct a $N_r N_t \times 1$ column channel vector $\boldsymbol{h}_b = \mathrm{vec}(\boldsymbol{H}_b)$. The beamspace channel covariance matrix is $\boldsymbol{\Sigma}_b = E[\boldsymbol{h}_b \boldsymbol{h}_b^H]$. $\boldsymbol{H}_b$ is sparse due to the mm-wave propagation characteristics [1], [3], [14] and the channel power is concentrated in a low-dimensional sub-matrix. Let $\boldsymbol{\Sigma}_{b,k}$ denote the channel covariance matrix for the k^{th} cell and $\sigma_k^2 = \mathrm{tr}(\boldsymbol{\Sigma}_{\mathrm{b,k}})$ the total channel power. For each cell, define the following sets of indices as the *channel sparsity masks*, $\mathcal{M}_k$, that capture most of the channel power:

$$\mathcal{M}_k = \{i : \boldsymbol{\Sigma}_{b,k}(i,i) \geqslant \gamma_k \max_i \boldsymbol{\Sigma}_{b,k}(i,i)\} \ , \ \mathcal{M} = \bigcup_{k=1,\cdots,K} \mathcal{M}_k \tag{12}$$

where the threshold γ_k is chosen so that $\mathcal{M}_k$ captures a specified (large) fraction $\eta_k \in [0,1]$ of the channel power

$$\sum_{i\in\mathcal{M}_k} \boldsymbol{\Sigma}_{b,k}(i,i) \geq \eta_k \sigma_k^2 \ . \tag{13}$$

$\mathcal{M}_k$ and $\mathcal{M}$ represent the *channel sparsity masks or signatures* for the k^{th} cell and entire area. For the k-th cell, the low-dimensional channel covariance matrix is defined as

$$\tilde{\boldsymbol{\Sigma}}_{b,k} = [\boldsymbol{\Sigma}_{b,k}(i,j)]_{i,j\in\mathcal{M}_k}. \tag{14}$$

B. Measurement Model and Empirical Channel Statistics

In practice, channel statistics are estimated from noisy measurements. We consider the following model for the beamspace channel measurements:

$$\boldsymbol{h}_{bn} = \sqrt{\mathcal{E}} \boldsymbol{h}_b + \boldsymbol{w}_b \tag{15}$$

where $\boldsymbol{h}_{bn}$ the noisy measurement vector, $\boldsymbol{w} \sim \mathcal{CN}(\boldsymbol{0}, \boldsymbol{I})$ denotes the noise vector, and $\mathcal{E}$ represents the signal-to-noise ratio (SNR). In (15), $\boldsymbol{h}_b$ represents a *normalized channel vector* so that $\sigma^2 = E[\|\boldsymbol{h}_b\|^2] = 1$. This is because we want to eliminate the influence of channel power on classification performance - we focus on the influence of *power distribution* over the sparsity masks. Thus, for the k-th cell we have:

$$\boldsymbol{\Sigma}_{bn,k} = E[\boldsymbol{h}_{bn} \boldsymbol{h}_{bn}^H] = \frac{\mathcal{E}}{\sigma_k^2} \boldsymbol{\Sigma}_{b,k} + \boldsymbol{I} \ . \tag{16}$$

For estimating $\boldsymbol{\Sigma}_{b,k}$, we choose N_{sp} sample MS positions, $\{(x_{r,i}, y_{r,i}) : i = 1, \cdots, N_{sp}\}$, uniformly placed within the k-th cell and use the empirical covariance matrix:

$$\hat{\boldsymbol{\Sigma}}_{b,k} = \frac{1}{N_{sp}} \sum_{i=1}^{N_{sp}} \boldsymbol{h}_b(x_{r,i}, y_{r,i}) \boldsymbol{h}_b^H(x_{r,i}, y_{r,i}) \tag{17}$$

where the channel vectors for different positions are generated using the physical model in Sec. II-A. We note that $E[\hat{\boldsymbol{\Sigma}}_{b,k}] = \boldsymbol{\Sigma}_{b,k}$ and the definition of sparsity masks $\mathcal{M}_k$ in (12) assumes high-SNR channel measurements.

IV. User Localization Algorithm

We now formulate the user localization problem, characterize the ML classifier, and low-dimensional classifier based on channel sparsity masks.

A. Maximum Likelihood Classifier

Suppose that the MS is located in one of the K disjoint cells with equal probability. The localization problem can be cast as a K-ary hypothesis testing problem

$$\mathrm{H}_k : \boldsymbol{h}_{bn} \sim \mathcal{CN}(0, \boldsymbol{\Sigma}_{bn,k}) \tag{18}$$

where $\boldsymbol{h}_{bn}$ is the noisy channel measurement (15) and $\boldsymbol{\Sigma}_{bn,k}$ is the covariance matrix for the k^{th} cell, as in (16). The optimal ML classifier chooses the cell as [15]:

$$C(\boldsymbol{h}_{bn}) = \arg \max_{k=1,\cdots,K} p_k(\boldsymbol{h}_{bn}) \tag{19}$$

where $p_k(\boldsymbol{h}_{bn})$ is the probability density function under H_k:

$$p_k(\boldsymbol{h}_{bn}) = \frac{1}{\pi^{N_r N_t} |\boldsymbol{\Sigma}_{bn,k}|} e^{-\boldsymbol{h}_{bn}^H \boldsymbol{\Sigma}_{bn,k}^{-1} \boldsymbol{h}_{bn}} \tag{20}$$

Using log-likelihood, the classifier can be simplified as

$$C(\boldsymbol{h}_{bn}) = \arg \min_{k=1} \left[\log(|\boldsymbol{\Sigma}_{bn,k}|) + \boldsymbol{h}_{bn}^H \boldsymbol{\Sigma}_{bn,k}^{-1} \boldsymbol{h}_{bn} \right] \tag{21}$$

B. Low-dimensional Classifier

The low-dimensional classifier exploits the sparsity patterns and operates on the low-dimensional channel vector defined by $\mathcal{M}$: $\tilde{\boldsymbol{h}}_{bn} = [\boldsymbol{h}_{bn}(i)]_{i\in\mathcal{M}}$. The classifier is given by (21) by replacing $\boldsymbol{\Sigma}_{bn,k}$ with $\tilde{\boldsymbol{\Sigma}}_{bn,k} = [\boldsymbol{\Sigma}_{bn,k}(i,j)]_{i,j\in\mathcal{M}_k}$. In a simpler version, used in the numerical results, the low-dimensional covariance matrices are defined with respect to the common mask $\mathcal{M}$: $\tilde{\boldsymbol{\Sigma}}_{bn,k} = [\boldsymbol{\Sigma}_{bn,k}(i,j)]_{i,j\in\mathcal{M}}$.

C. Classifier Performance Evaluation

We evaluate the classifier performance in terms of the average error probability:

$$P_e = \frac{1}{K}\sum_{k=1}^{K} P_{e,k}\ ,\ P_{e,k} = P(C(\boldsymbol{h}_{bn}) \neq k\,|H_k) \qquad (22)$$

where $P_{e,k}$ is the conditional error probability under H_k. We use Monte Carlo simulation to estimate P_e.

V. Numerical Results

We present three sets of numerical results. The first set shows the beamspace channel masks for different cells. The second shows impact of physical environment and system parameters on the localization performance. Finally, the performance of low-dimensional classifiers is discussed.

A. Beamspace Channel Statistics and Masks

Consider a MIMO system with $N_r = 25$ (BS) and $N_t = 5$ (MS), and antenna gains G_r and G_t that are proportional to N_r and N_t. The propagation frequency f_c is 38GHz [2]. We partition the MS movement region R into 16 disjoint cells of size $25m \times 25m$, and number them as in Fig. 2. For each cell, we calculate the path loss of NLoS paths via (8), and set the power of LoS path, $|\beta_{los}|^2$, $10dB$ larger than the average power of all NLoS paths within the cell. In each cell, we uniformly pick $N_{sp} = 10000$ sample MS positions and compute the average channel power, and covariance matrix for this cell by (17). This is used for generating normalized channel measurements as in (15). The channel sparsity masks with different threshold values are generated using (12). Fig. 3 shows $\mathcal{M}_k$ for cells 1, 4, 13, 16 which are at corners of the MS movement area, corresponding to $\gamma_k = \gamma = 0.1$. The shaded bins represent the dominant beamspace channel entries corresponding to pairs of BS/MS beams that are strongly coupled. The mask dimensions and patterns depend on the choice of γ and the physical environment.

B. MS Localization Performance

We next evaluate the influence of physical propagation environment, cell size, and MIMO dimensions on performance.

1) Physical Propagation Environment: We first discuss the impact of the number of paths N_p. We set the cell size to $25m \times 25m$ (total 16 cells) and consider a system with $N_t = 5$ (MS) and $N_r = 25$ (BS). We evaluate P_e as a function of SNR for different values of N_p by progressively adding extra scatterer positions to previous locations. Fig. 4a shows that P_e first decreases as N_p is increased from 5 to 10, but then P_e increases when N_p is increased to 50 and 100. This illustrates that for given system dimensions, too many paths can degrade performance as channel signatures for different cells start looking similar.

2) MIMO Dimensions: Fig. 4b-4c show that systems with larger number of antennas can exploit an environment with larger number of paths for improved performance. In practice, increasing the number of antennas at the MS is costly. So we only increase the number of BS antennas N_r. We fix MS with $N_t = 5$ and vary $N_r = 10, 25, 60$. In Fig. 4b, $N_p = 5$ (very sparse environment), and increasing N_r does not change performance. However, in 4c, $N_p = 100$ (much richer environment) and now increasing N_r results in significantly improved performance. We note that the channel dimension $N_t N_r$ increases as $50, 125, 300$ and is comparable to $N_p = 100$ in this case. On the other hand, $N_p = 5$ is much smaller than the channel dimension in Fig. 4b.

3) Cell Size: The size of each cell represents the localization resolution. Fig. 5a shows the localization performance for different cell sizes within the fixed $100m \times 100m$ target moving area, with $N_t = 5$, $N_r = 25$ and $N_p = 5$ scatterers. Surprisingly, at sufficiently high SNR, P_e does not increase much at all as we decrease the cell size from $25m \times 25m$ to $5m \times 5m$. This is promising and warrants further investigation.

C. Low-Dimensional Classifier

We examine the performance of the low-dimensional classifier relative to the full-dimensional classifier in Figs. 5b-5c. The dimensionality reduction is controlled by the threshold γ in (12). We illustrate with three values of $\gamma = 0.2, 0.3, 0.4$ for two different values of N_p. Fig. 5b corresponds to $N_p = 5$ (sparse environment) and the results show that there is relatively little loss in performance even with the most drastic dimension reduction from 125 to 11. Fig. 5c shows the results for $N_p = 10$ and in this case, there is more significant loss in performance with dimension reduction due to larger number of paths. However, still the classifier corresponding to $\gamma = 0.2$ yields quite competitive performance compared to the full-dimensional classifier: the P_e increases by a factor of 2 whereas the dimension is reduced by a factor of 60, resulting in a very significant reduction in complexity. These initial performance results indicate that by exploiting beamspace channel sparsity, dramatic reductions in complexity are possible with relatively small loss in performance.

VI. Conclusions

We have a proposed a modeling framework for sparse high-dimensional MIMO channels encountered in massive MIMO and mm-wave systems, and discussed an application to MS localization based on sparse beamspace channel signatures. Beamspace MIMO offers a promising approach to high-dimensional system design as the channel sparsity is naturally manifested in beamspace. We discussed the sparse structure of the beamspace channel covariance matrix, and introduced the *channel sparsity mask* to capture the low-dimensional channel subspace that carries most of the power and MS location information. A ML classifier for MS localization is proposed assuming Gaussian channel statistics. Low-dimensional classifier design is also proposed using the sparsity masks. Numerical results are provided to illustrate the impact of physical environment and system parameters on performance. In particular, the results indicate that our approach offers a promising framework for optimizing the *performance-complexity tradeoffs* that are inherent to high-dimensional (massive) MIMO systems. Ongoing work includes: extending the framework to include path delay information as well as two-dimensional arrays for a full 3D model, and relaxing the assumption of a MS always facing the BS, which may be feasible in some scenarios in which a user intentionally points

(a) (b) (c) (d)

Fig. 3: Channel sparsity masks: (a): $\mathcal{M}_1$, (b): $\mathcal{M}_4$, (c): $\mathcal{M}_{13}$, and (d): $\mathcal{M}_{16}$.

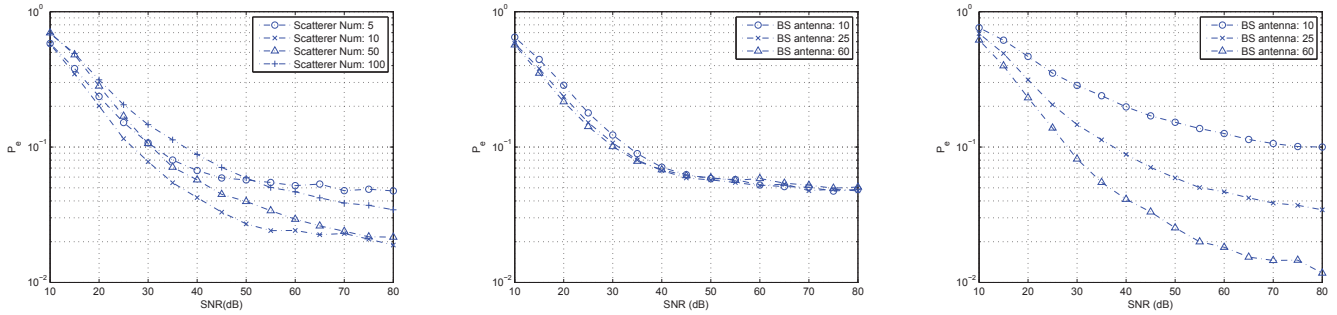

(a) (b) (c)

Fig. 4: (a) P_e for different N_p with $N_r = 25$, $N_t = 5$. (b): P_e for $N_t = 5$ and different N_r in an environment with $N_p = 5$. (c): P_e for $N_t = 5$ and different N_r in an environment with $N_p = 100$.

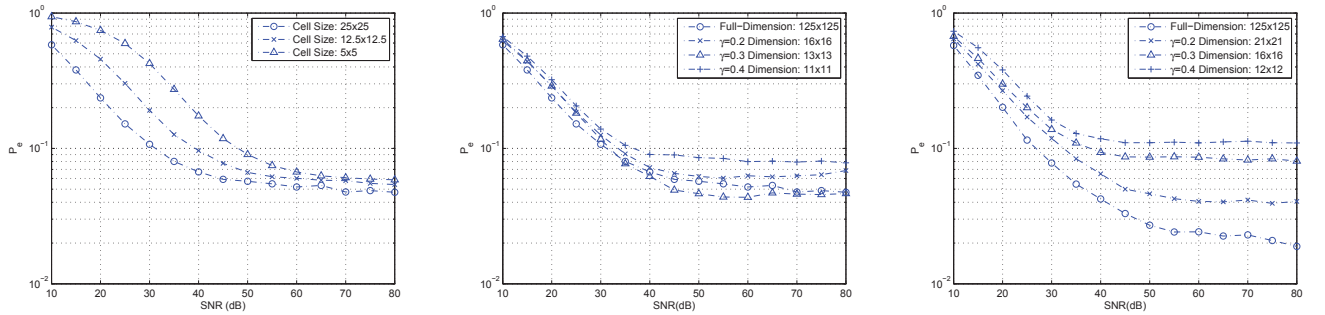

(a) (b) (c)

Fig. 5: (a): P_e for different cell sizes with $N_r = 25$, $N_t = 5$ and $N_p = 5$. (b): P_e of low-dimensional classifiers for system with $N_r = 25$, $N_t = 5$ and $N_p = 5$. (c): P_e of low-dimensional classifiers for $N_r = 25$, $N_t = 5$ and $N_p = 10$.

the MS towards a BS. Our ultimate goal is to develop methods that do not require such user cooperation.

REFERENCES

[1] Z. Pi and F. Khan, "An introduction to millimeter-wave mobile broadband systems," *IEEE Personal Comm.*, vol. 49, pp. 101–107, June 2011.

[2] T. S. Rappaport, E. Ben-Dor, J. N. Murdock, and Y. Qiao, "38GHz and 60GHz angle-dependent propagation for cellular & peer-to-peer wireless communications," in *2012 IEEE International Conf. on Comm.*, 2012, pp. 4568–4573.

[3] G.-H. Song, J. Brady, and A. Sayeed, "Beamspace mimo transceivers for low-complexity and near-optimal communication at mm-wave frequencies," in *2013 IEEE International Conf. on Acoustics, Speech and Signal Processing*. IEEE, 2013, pp. 4394–4398.

[4] A. M. Sayeed and N. Behdad, "Continuous aperture phased MIMO: Basic theory and applications," in *48th Annual Allerton Conf. on Coomunications, Control and Computing*, Sept.29-Oct.1 2010, pp. 1196–1203.

[5] ——, "Continuous aperture phased MIMO: A new architecture for optimum line-of-sight links," in *IEEE International Symposium on Antennas and Propagation*, July 2011, pp. 293–296.

[6] J. Brady, N. Behdad, and A. M. Sayeed, "Beamspace MIMO for millimeter-wave communications: System architecture, modeling, analysis and measurements," *IEEE Trans. on Antennas and Propagation*, vol. 50, no. 10, pp. 2563–2579, 2002.

[7] T. S. Rappaport, J. H. Reed, and B. D. Woerner, "Position location using wireless communications on highways of the future," *IEEE Communications Magazine*, vol. 34, October 1996.

[8] C. K. Seow and S. Y. Tan, "Non-line-of-sight localization in multipath environment," *IEEE Trans. on Mobile Computing*, vol. 7, 2008.

[9] H. Miao, K. Yu, and M.J.Juntti, "Positioning for NLOS propagation: Algorithm derivations and cramer-rao bounds," *IEEE Trans. on Vehicular Technology*, vol. 56, 2007.

[10] T. Roos, P. Myllymaki, and H. Tirri, "A statistical modeling approach to location estimation," *IEEE Trans. on Mobile Computing*, vol. 1, 2002.

[11] K. Papakonstantinou and D. Slock, "Performance bounds and identifiability conditions for location estimation in NLoS dynamic environments," in *2011 IEEE Statistical Signal Processing Workshop (SSP)*, June 2011, pp. 189–192.

[12] A.Goldsmith, *Wireless Communications*. Cambridge Univ. Press, 2006.

[13] A. M. Sayeed, "Deconstructing multiantenna fading channels," *IEEE Trans. on Signal Processing*, vol. 50, no. 10, pp. 2563–2579, 2002.

[14] E. Torkildson, H. Zhang, and U. Madhow, "Channel modeling for millimeter wave MIMO," in *Information Theory and Applications Workshop*, 2012, pp. 1–8.

[15] S. M. Kay, *Fundamentals of Statistical Signal Processing: Estimation Theory*, 1993, vol. 1.